SRPK3 Is Essential for Cognitive and Ocular Development in Humans and Zebrafish, Explaining X-Linked Intellectual Disability

Arkaprava Roychaudhury, MS,[1†] Yu-Ri Lee, PhD,[1†] Tae-Ik Choi, PhD,[1†] Mervyn G. Thomas, MD, PhD,[2†] Tahir N. Khan, PhD,[3] Hammad Yousaf, MS,[3] Cindy Skinner, BSN, RN,[4] Gail Maconachie, PhD,[2,5] Moira Crosier, HNC,[6] Holli Horak, MD,[7] Cris S. Constantinescu, MD, PhD, FRCP,[8,9] Tae-Yoon Kim, PhD,[1] Kang-Han Lee, PhD,[1] Jae-Jun Kyung, MS,[1] Tao Wang, PhD,[10] Bonsu Ku, PhD,[11] Bernard N. Chodirker, MD,[12] Michael F. Hammer, PhD,[13] Irene Gottlob, MD, PhD,[2,9] William H. J. Norton, PhD,[14] Robert Gerlai, PhD,[15] Hyung-Goo Kim, PhD,[16] Claudio Graziano, MD,[17] Tommaso Pippucci, PhD,[18] Emanuela Iovino, PhD,[18] Francesca Montanari, MD,[18] Giulia Severi, MD,[18] Camilo Toro, MD,[19] Cornelius F. Boerkoel, MD, PhD,[19] Hyo Sun Cha, BS,[20] Cheol Yong Choi, PhD,[20] Sungjin Kim, PhD,[21] Je-Hyun Yoon, PhD,[22] Kelly Gilmore, MS,[23] Neeta L. Vora, MD,[23] Erica E. Davis, PhD,[3,24] Albert E. Chudley, MD,[12] Charles E. Schwartz, MD, PhD,[4,25] and Cheol-Hee Kim, PhD[1]

Objective: Intellectual disability is often the outcome of neurodevelopmental disorders and is characterized by significant impairments in intellectual and adaptive functioning. X-linked intellectual disability (XLID) is a subset of these disorders caused by genetic defects on the X chromosome, affecting about 2 out of 1,000 males. In syndromic form, it leads to a broad range of cognitive, behavioral, ocular, and physical disabilities.

Methods: Employing exome or genome sequencing, here we identified 4 missense variants (c.475C > G; p.H159D, c.1373C > A; p.T458N, and c.1585G > A; p.E529K, c.953C > T; p.S318L) and a putative truncating variant (c.1413_1414del; p.Y471*) in the *SRPK3* gene in 9 XLID patients from 5 unrelated families. To validate *SRPK3* as a novel XLID gene, we established a knockout (KO) model of the *SRPK3* orthologue in zebrafish.

Results: The 8 patients ascertained postnatally shared common clinical features including intellectual disability, agenesis of the corpus callosum, abnormal eye movement, and ataxia. A ninth case, ascertained prenatally, had a complex structural brain phenotype. Together, these data indicate a pathological role of *SRPK3* in neurodevelopmental disorders. In post-fertilization day 5 larvae (free swimming stage), KO zebrafish exhibited severe deficits in eye movement and swim bladder inflation, mimicking uncontrolled ocular movement and physical clumsiness observed in human patients. In adult KO zebrafish, cerebellar agenesis and behavioral abnormalities were observed, recapitulating human phenotypes of cerebellar atrophy and intellectual disability.

Interpretation: Overall, these results suggest a crucial role of *SRPK3* in the pathogenesis of syndromic X-linked intellectual disability and provide new insights into brain development, cognitive and ocular dysfunction in both humans and zebrafish.

ANN NEUROL 2024;00:1–18

Intellectual disability, characterized by limited intellectual functioning, affects approximately 1–3% of the global population.[1] Males are more commonly affected by intellectual disability than females by 20–30%, likely due to an enrichment of genes on the X-chromosome that are required for neurodevelopment. X-linked intellectual disability (XLID), resulting from hemizygous variants, is a significant contributor to intellectual disability seen in males.[2] This chronic condition is present from birth, and continues throughout an individual's life. Consequently, it necessitates sustained family engagement, medical care and social services, which imposes an enormous burden on both the families and society. Researchers worldwide have identified 145 XLID genes that contribute to 114 XLID syndromes and 63 non-syndromic XLID entities. Exome sequencing has accelerated mutational analysis of the coding regions of the X-chromosome, resulting in the identification of 28 of the 145 XLID genes in the past decade.[3] However, the genotypic and phenotypic heterogeneity of intellectual disability is significant, and current estimates suggest that the number of genes linked to intellectual disability is over 1,500.[4] With the complete sequence of the X chromosome coupled with the capability of next-generation sequencing and functional analysis, there is an exciting opportunity to better understand the genetic bases for this group of disorders.

Through exome sequencing, we initially identified a missense variant in *SRPK3* (serine/arginine-rich protein-specific kinase 3) in an XLID family. The variant was inherited from a Manitoba mother of Anglo-Saxon origin. Subsequently, we discovered a second variant identified by the Undiagnosed Disease Program (UDP) at the NIH in the United States. Given the presence of 2 missense variants in *SRPK3*, we conducted a search of a database generated by our previous Sanger X-chromosome resequencing project,[5] which revealed a third missense variant. Further data sharing identified unrelated pediatric and fetal male cases harboring missense and nonsense *SRPK3* variants, respectively. Combined together, the identification of these rare variants made *SRPK3* a compelling candidate gene for in-depth analysis as a novel XLID gene. *SRPK3* is known to specifically phosphorylate serine-arginine (SR) proteins which act as splicing factors.[6] Phosphorylation is required for SR proteins to enter the nucleus and play a role in alternative splicing of pre-mRNA, mRNA export, and other processing events. Recently, new functions of SRPK2 were reported in synaptic vesicle and neurotransmitter release.[7] Although our bioinformatic analysis predicted that the 3 variants were likely pathogenic and related to the XLID phenotypes in the families, further investigation was required to confirm these predictions and elucidate the molecular mechanisms underlying the observed XLID phenotype.

Protein modeling and in vitro subcellular localization experiments were employed to assess the potential impact of missense variants on the structure and function of *SRPK3*. Furthermore, to investigate *SRPK3* as a novel XLID gene, a knockout (KO) zebrafish model of *srpk3* was generated and evaluated at different developmental stages to understand how *SRPK3* deficiency adversely affected its function in vivo.

View this article online at wileyonlinelibrary.com. DOI: 10.1002/ana.27037

Received May 30, 2023, and in revised form Jul 7, 2024. Accepted for publication Jul 8, 2024.

Address correspondence to Dr Charles E. Schwartz, Greenwood Genetic Center, Greenwood, SC 29646. E-mail: charles.schwartz224@gmail.com
Dr Cheol-Hee Kim, Department of Biology, Chungnam National University, Daejeon 34134, Korea. E-mail: zebrakim@cnu.ac.kr

[†]These authors contributed equally to this work.

From the [1]Department of Biology, Chungnam National University, Daejeon, South Korea; [2]The University of Leicester Ulverscroft Eye Unit, Department of Neuroscience, Psychology and Behavior, University of Leicester, Leicester, UK; [3]Stanley Manne Children's Research Institute, Ann & Robert H. Lurie Children's Hospital of Chicago, Chicago, IL, USA; [4]Greenwood Genetic Center, Greenwood, SC, USA; [5]Division of Ophthalmology and Orthoptics, Health Science School, University of Sheffield, Sheffield, UK; [6]Human Developmental Biology Resource, Biosciences Institute, Faculty of Medical Sciences, Newcastle University, Newcastle upon Tyne, UK; [7]Department of Neurology, University of Arizona, Tucson, AZ, USA; [8]Academic Unit of Mental Health and Clinical Neuroscience, University of Nottingham, Nottingham, UK; [9]Cooper Neurological Institute and Cooper Medical School of Rowan University, Camden, NJ, USA; [10]McKusick-Nathans Department of Genetic Medicine, Johns Hopkins University, Baltimore, MD, USA; [11]Disease Target Structure Research Center, Korea Research Institute of Bioscience and Biotechnology, Daejeon, South Korea; [12]Department of Pediatrics and Child Health, Max Rady College of Medicine, Rady Faculty of Health Sciences, University of Manitoba, Winnipeg, MB, Canada; [13]BIO5 Institute, University of Arizona, Tucson, AZ, USA; [14]Department of Genetics and Genome Biology, University of Leicester, Leicester, UK; [15]Department of Psychology, University of Toronto Mississauga, Mississauga, ON, Canada; [16]Neurological Disorders Research Center, Qatar Biomedical Research Institute, Hamad Bin Khalifa University, Doha, Qatar; [17]Medical Genetics Unit, AUSL Romagna, Cesena, Italy; [18]IRCCS Azienda Ospedaliero-Universitaria di Bologna, Bologna, Italy; [19]NIH Undiagnosed Diseases Program, NIH Office of Rare Diseases Research and NHGRI, Bethesda, MD, USA; [20]Department of Biological Sciences, Sungkyunkwan University, Suwon, South Korea; [21]Department of Microbiology & Molecular Biology, Chungnam National University, Daejeon, South Korea; [22]Department of Oncology Science, University of Oklahoma, Oklahoma City, OK, USA; [23]Division of Maternal Fetal Medicine, Department of Ob/Gyn, University of North Carolina at Chapel Hill, Chapel Hill, NC, USA; [24]Department of Pediatrics, Cell and Developmental Biology, Feinberg School of Medicine, Northwestern University, Chicago, IL, USA; and [25]Department of Pediatrics and Human Development, College of Human Medicine, Michigan State University, Grand Rapids, MI, USA

Additional supporting information can be found in the online version of this article.

Materials and Methods

Further details about the procedures are described in Supplementary Methods.

The human subject research protocol for the study was approved by the Institutional Review Boards (IRBs). Informed consent was obtained from all study participants and/or their parents or legal guardians. Participants, enrolled in the Greenwood Genetic Center XLID study, were evaluated by clinical geneticists and other specialists, and underwent comprehensive laboratory analyses for intellectual disability. All postnatal patients were found to have a normal karyotype and negative molecular readout for Fragile X syndrome. The prenatal case had a normal male microarray per standard of care genetic testing in the setting of a fetal structural abnormality. Given that each center independently identified *SRPK3* as the novel candidate gene for intellectual disability or neurodevelopmental disorder, the enrichment kits used and sequencing protocols varied between centers.

Family 1 (K8765, GGC)

Patients with XLID and neurotypical control males were enrolled by the Greenwood Genetic Center (GGC), USA for their study of XLID. X-chromosome exome sequencing on probands from XLID families was conducted using a TruSeq Genomic DNA Library Preparation kit, a SureSelect Target Enrichment kit, and the HiSeq2000. Bowtie2 and Unified Genotyper were used for alignment, base recalibration, and variant calling. Sanger sequencing was used for validation, segregation analysis, and polymorphism studies.

Family 2 (UDP, NIH)

After identification of the first variant, we subsequently became aware of a second variant identified by the UDP at NIH, USA. Quartet exome sequencing was performed for identification and verification of the variant. Image analysis and base calling were performed using Illumina Genome Analyzer Pipeline software. Reads were aligned to a human reference sequence using a package called Efficient Large-scale Alignment of Nucleotide Databases (Illumina, San Diego, CA, USA).

Family 3 (UAGC)

Clinical information on males of family 3 was collected by the University of Arizona and molecular data was obtained by the Genomics Core (UAGC), USA. Whole exome sequencing was performed twice on 4 samples from the family using different enrichment kits. Variants were annotated and candidate X-linked variants were identified by comparing the genotype of the male proband to that of the mother and father. A prioritizing system was implemented to identify true X-linked variants, and those within the highest priority level were validated by Sanger sequencing. Variants with a frequency <3% in the ESP were also screened for de novo mutations in the proband that were not observed in the 1,000 genomes or ESP datasets were also examined. *SRPK3* variants are reported as per Human Genome Variation Society (HGVS) guidelines against the accession ID: NM_014370.4.

Family 4 (IRCCS AOUBO)

Whole genome sequencing (WGS) was performed on male proband and parents from family 4 as part of a research project applying WGS to the genetic characterization of syndromic intellectual disability. As ID appeared in this family as a sporadic disease affecting a young male born to unaffected parents, prioritization of variants as candidate for association with ID followed de novo occurrence, autosomal recessive and X-linked inheritance. Protein-altering variants with damaging potential defined as a CADD Phred-score higher than 15 and extremely low allele frequency in the population (<0.0001 in gnomAD whole genome dataset) were examined as prominent candidates.

Family 5 (UNC-Chapel Hill; Prenatal Case)

Fetus-parent trio WGS was performed as part of a research project on fetal brain abnormalities. We performed library prep with 2 × 150 bp reads on an Illumina NovaSeq 6,000 platform. Analysis using the Franklin variant interpretation platform (Genoox, Tel Aviv, Israel; version 68.1, https://franklin.genoox.com/) was used to filter for rare (allele frequency <0.01) non-synonymous, exonic or splice variants and indels (±10 nucleotides from splice junction) and structural variations affecting the coding regions of the genome that segregated with disease in de novo, autosomal recessive, X-linked, or maternal mitochondrial DNA inheritance patterns. The *SRPK3* variant was Sanger confirmed in the CLIA molecular laboratory.

Expression Studies for Protein and mRNA

Human embryonic samples were collected with appropriate maternal consents and ethical approval by NRES Committee North East-Newcastle & North Tyneside 1. Spatiotemporal *SRPK3* brain expression was investigated by immunohistochemistry on human embryonic tissue as described previously.[8] The embryonic development stage was determined by external morphology assessment as previously described.[9,10] We analyzed the developmental transcriptome datasets from the BrainSpan project,[11,12] specifically examining spatiotemporal expression of *SRPK3* mRNA in the developing prenatal and post-natal brain. Details regarding transcriptome profiling is available at www.brainspan.org.

Zebrafish Husbandry

A closed line of wild-type (WT) zebrafish (*Danio rerio*) maintained in our animal facility were reared under specific environmental conditions. All experiments were conducted with approval from the Institutional Animal Care and Use Committees (IACUC) of Chungnam National University (202012A-CNU-170). Zebrafish used in the experiment were obtained from the Zebrafish Center for Disease Modeling (ZCDM; South Korea).

Whole Mount In Situ Hybridization and Histological Analysis

Whole-mount in situ hybridization (WISH) was performed using a protocol described previously.[13] The fixed embryos were

dehydrated with MeOH, rehydrated, and permeabilized with Proteinase K. RNA (XM_689881.9) probe was synthesized in vitro using a cloned amplicon and then dissolved in HYB+ solution for use in the experiment. The antisense RNA probe was added to the embryos and allowed to hybridize overnight. The larvae were then washed and incubated with an anti-DIG Fab fragment conjugated with alkaline phosphatase. For histological analysis, paraffin sections of the adult zebrafish brain were stained with hematoxylin and eosin (H&E) staining.

Subcellular Localization of SRPK3 Variants in HeLa Cells

SRPK3 WT and variants (H159D, S318L, T458N, and E529K) were amplified through polymerase chain reaction (PCR) and subsequently inserted into the *Xho*I and *Xba*I sites of the pEGFP-C3 vector. HeLa cells were transfected with each plasmid encoding *GFP-SRPK3* WT or variants. Transfected cells were fixed in 3% paraformaldehyde/PBS and permeabilized in 0.1% Triton X-100/PBS. After blocking with 2% BSA, cells were stained with DAPI (4′,6-diamidino-2-phenylindole) for 25 min at room temperature. Confocal imaging was performed using a Zeiss LSM700 microscope, and acquired images were processed with ZEN 3.2. For the detection of *GFP-SRPK3* in the Western blotting, antibodies were used as follows: mouse polyclonal anti-greeen fluorescent protein (GFP) (Clontech, 632,381, 1:2,000) and rabbit recombinant monoclonal anti-GAPDH (Bethyl, BLR103H, 1:10,000).

Generation of srpk3 KO Zebrafish Model Using CRISPR/Cas9

The gene sequences for zebrafish *srpk3* were obtained from the ENSEMBL database (ENSDARG00000005916), and primers were designed for in vitro transcription of sgRNAs targeting *srpk3*. Cas9 expression vector pT3TS-nCas9n was used to synthesize Cas9 mRNA, which was injected along with sgRNAs into 1-cell stage zebrafish embryos. Mutations were validated using T7E1 assay, and founder (F0) fish were raised to adulthood and out-crossed with WT zebrafish to generate germ line mutations. The F1 generation was raised to adulthood, and individuals with the heterozygous genotype were in-crossed to produce stable homozygous *srpk3* KO zebrafish lines (F2).[14]

Generation of SRPK3 Plasmids and In Vitro Transcription

We obtained a full-length WT human *SRPK3* construct (GenBank: NM_014370.4) and subcloned it into the pCS2+ vector. Subsequently, we generated variant constructs using site-directed mutagenesis.[15] We designed primers carrying the mutated nucleotide and used the WT *SRPK3* ORF construct as a template for PCR amplification. After subjecting the amplified product to *Dpn*I digestion for the selective digestion of the methylated WT template, variant colonies were acquired through cloning. The Sanger sequencing method was employed to confirm the sequences of both the WT and variant constructs. Using the mMessage mMachine Sp6 transcription kit (ThermoFisher Scientific, Waltham, Massachusetts, USA), we generated capped mRNA by utilizing the linearized pCS2+ vector as a template. We used 200, 250, and 500 pg of synthesized mRNA for overexpression and functional validation studies.

Quantification of mRNA Expression Level by Real-Time qRT-PCR

Total RNA was isolated from WT and *srpk3* KO adult zebrafish brain. Real-time qRT-PCR was performed in triplicates using SsoAdvanced Universal SYBR Green Supermix (BioRad, California, USA) on a PCRmax Eco 48 Real-Time qPCR System (PCRmax, Staffordshire, United Kingdom). Cq values were automatically calculated on PCRmax Eco software. Data were analyzed using the ΔΔCq method: Cq values were averaged, then subtracted to the average Cq value of *ef1α* (ΔCq), and last the fold change was determined using the formula $2^{-(^{\Delta Cq}\text{sample} - {}^{\Delta Cq}\text{reference})}$. A housekeeping gene *ef1α* was used as endogenous RNA control.

Analysis of Spontaneous Eye Movements in KO Zebrafish

Zebrafish larvae were maintained at a constant temperature of 28.5°C until they reached 5 dpf, a developmental stage commonly used for spontaneous eye movement. At 5 dpf, the zebrafish larvae were mounted on a petri dish using 2% low melting agarose, and a 3-min video of their eye movements was recorded using a brightfield microscope. The recorded video was then analyzed using MATLAB software to track and quantify the eye movements of the zebrafish larvae.[16]

Social Interaction Assay in Adult KO Zebrafish

The social interaction assay[17] involved observing the behavior of zebrafish in a divided tank (24 × 15 × 15 cm) consisting of 2 sections. One section was designated for the conspecific stimulus fish and the other for the experimental fish. Three zebrafish were introduced as stimulus fish also called social cue. The tank was further divided into 4 equal areas (zone 1, 2, 3, and 4). Zone 1 was the nearest to the social stimulus, followed by zone 2, zone 3, and zone 4. A 15-min video recording was made, and the behavior was subsequently analyzed using Ethovision XT video-tracking software (Noldus, The Netherlands). All trials were conducted from 1,300 to 1,700 hours.

Shoaling Bowl Assay in Adult KO Zebrafish

The shoaling bowl assay[17] was used to access whether *srpk3* KO zebrafish modified shoaling (group forming) behavior. Three animals of the same genotype were placed in a bowl (upper half diameter, 33 cm; bottom diameter, 24 cm; height, 11 cm; and water depth, 3.2 cm) and a top-view video was taken by Sony HDR-CX190 camera for 15 min. The mean distance between individual fish was analyzed using Ethovision XT software (Noldus, The Netherlands). All trials were conducted from 1,300 to 1700 hours.

Statistical Analysis

Statistical analysis was performed using GraphPad Prism 8. The data were presented as mean ± standard error of the mean (SEM), with a p value of <0.05 being considered significant. For parametric statistical comparison of 2 groups, a 2-tailed

independent sample *t* test was performed, while for comparison involving more than 2 groups, 1-way analysis of variance (ANOVA) followed by Tukey's honestly significant difference (HSD) post-test was employed.

Results

Patient Information and Bioinformatic Analysis of SRPK3 *Variants*

Clinical information on males with the p.H159D and p.E529K *SRPK3* variants (NP_055185.2) had been provided by the Department of Pediatrics and Child Health at the University of Manitoba, Canada, and the University of Arizona Genomics Core (UAGC, USA) respectively, as part of our extensive study on XLID. All postnatal patients exhibited learning difficulties and intellectual disabilities. In 2 families, H159D and T458N, brain abnormalities were observed, including agenesis of the corpus callosum and cerebellar atrophy, respectively. These 2 families also had abnormal speech, while all 3 families exhibited mild intellectual disabilities, suggesting that the variants in *SRPK3* were relevant to XLID in these families. Intellectual disability-related features, including learning impairment and/or delayed language skills and/or poor attention span were present in the patients. Eye movement-related phenotypes, including abnormal smooth pursuit, convergence insufficiency, lazy eye, were also clinically described in all 4 patients (Table S1). Bioinformatic analysis predicted that the p.H159D, p.T458N, and p.E529K variants were very likely disease causing, and all 3 missense variants were found to segregate within the respective families. Among these variants, c.475C > G (NM_014370.4); p.H159D was identified in Family 1 by X-chromosome exome sequencing; c.1373C > A; p.T458N was identified in Family 2 at NHGRI; c.1585G > A; p.E529K was identified in Family 3; a maternally-inherited c.953C > T; p.S318L variant was identified in the proband of family 4; and a maternally-inherited c.1413_1414del; p.Y471* variant was identified by genome sequencing in the fetal proband of family 5. The minor allele frequency (MAF) of the reported *SRPK3* variants was evaluated using gnomAD. Our analysis revealed that the c.1585G > A variant exhibited a very low MAF (MAF = 0.0001), whereas c.475C > G, c.953C > T, c.1373C > A, and c.1413_1414del variants were not detected in the gnomAD dataset. All 5 variants had high CADD scores of: 24.8 (c.475C > G), 23.6 (c.953C > T), 24.4 (c.1373C > A), 25.5 (c.1585G > A), and 20.3 (c.1413_1414del), indicating a greater likelihood that these variants are deleterious.

Family 1 and 2: p.H159D, p.T458N (NM_014370.4)

The first variant c.475C > G; p.H159D in Family 1 was maternally inherited from a Manitoba female of Anglo-Saxon origin (Fig 1A). All males in the family presented with delayed motor, social, adaptive and language skills at an early age (Fig 1B). Family 1 was referred to the genetics clinic in Winnipeg, Manitoba, due to cognitive impairments in 5 males, ranging from mild to moderate severity. Although the pattern of inheritance was consistent with XLID, the etiology remained unknown. Brain imaging (x-ray, CT, and/or MRI scans) was performed on 4 of the 5 affected males, revealing irregular and asymmetrically dilated lateral ventricles

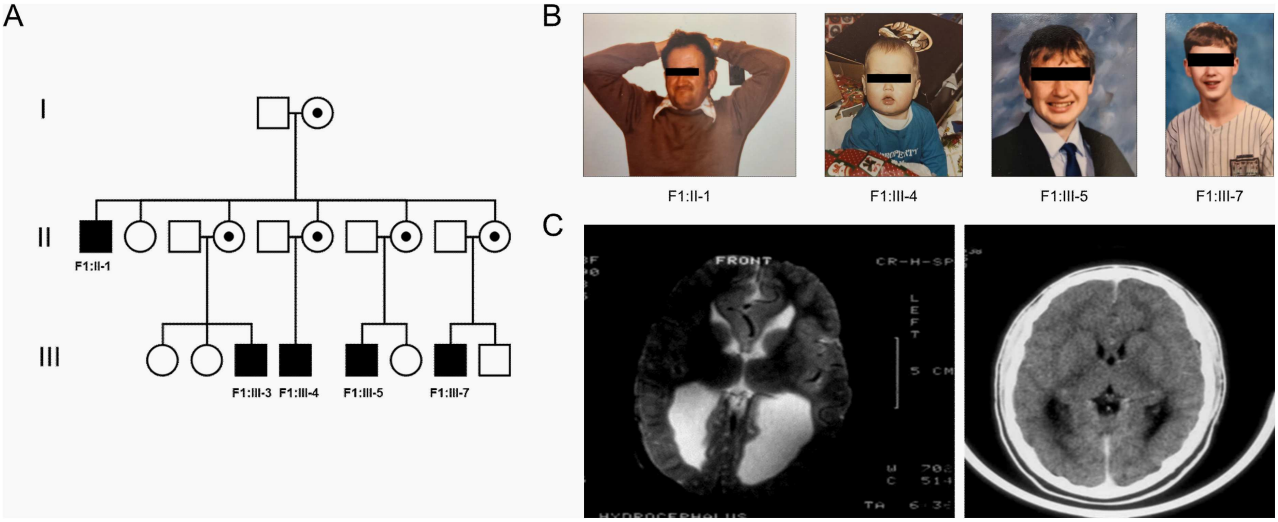

FIGURE 1: Pedigree of Family 1 demonstrating X-linked pattern of inheritance. (A) The first variant in the *SRPK3* gene (c.475C > G; p.H159D) was identified in 5 affected males (F1:II-1, F1:III-3, F1:III-4, F1:III-5, F1:III-7) from a well-established X-linked intellectual disability (XLID) family. (B) Photographs of 4 (F1:II-1, F1:III-4, F1:III-5, F1:III-7) affected males. (C) Brain imaging were performed on 4 of the 5 affected males. A representative MRI image of the patient F1:III-4, demonstrating a dilatation of the occipital horns.

in all 4 (Fig 1C). Three males demonstrated dilatation of the occipital horns (colpocephaly). Additionally, all 4 males exhibited varying degrees of agenesis and/or dysgenesis of the corpus callosum. In 1 male, there was moderate to severe white matter bulk loss. Patient F1:II-1 had a large head with a possible diagnosis of arrested hydrocephalus, whereas patient F1:III-5 had a mild delay in gross motor milestones—sitting at 8 months, walking at 18 months, and not speaking until after 3 years of age—in addition to poor attention span. Patient F1:III-4 also had a very short attention span, and his developmental profile was scattered with a delay in the cognitive area. However, none of the 4 affected males exhibited facial dysmorphic features or other visible malformations, and 3 males had macrocephaly. We excluded commonly known forms of X-linked disorder with these brain image findings during assessments conducted between 1984 and 2013, when this study was initiated. The second variant (p.T458N) in Family 2 was identified by the UDP at NHGRI, NIH. The proband F2 was 24-year-old man of Northern European origin with adult-onset progressive ataxia, dysarthria, decreased dexterity, tremor and vertigo with onset since age 21. Proband showed long standing history of learning difficulties with slow processing speed requiring special education, left eye exotropia, and rapid onset of a progressive ataxic syndrome (primarily truncal) beginning in his early 20s. A comprehensive evaluation for acquired toxic-metabolic, mitochondrial, immune-mediated, and genetic causes of ataxia was undertaken. Imaging of the brain revealed a pattern of rapidly progressing cerebellar atrophy (but not supratentorial atrophy) over a period of 3 years. The proband was identified with maternally inherited *SPRK3* c.1373C > A; p.T458N (Fig S1A).

Family 3: p.E529K

The proband (F3:III-1) in Family 3 is presented with intellectual disability, muscle hypotonia, and ataxia. Similar phenotypical characteristics were observed in his maternal uncle, who carried the hemizygous *SRPK3* variant. The proband's mother, heterozygous for the *SRPK3* variant, showed no symptoms (Fig S1B). Brain MRI was performed solely on the proband, revealing a bilateral and symmetric prominence of the posterior convexity sulci, displaying a mild posterior-to-anterior gradient. Additionally, mild bilateral symmetric reduction in parietal gyral white matter volumes was observed. Along with a loss of volume within the posterior body of the corpus callosum, possibly due to a decreasing volume in traversing fibers in that area.

Family 4: p.S318L

The proband in family 4 is a young boy who was evaluated at 7 and 18 months of age for a global developmental delay. He was born at term after an uneventful pregnancy, parents are Italian and not consanguineous. Family history is remarkable for the presence of a cousin (son of his mother's sister) who is reported to show a severe developmental delay. It was not possible to visit or test this child. He did not show facial dysmorphisms, his occipital frontal circumference (OFC) was in the normal range (43.5 cm at 7 months, 46 at 18), he had a high narrow palate, long slender fingers with hypermobility of small joints. He had a poor suck and failure to thrive from the age of 5 months. He had axial hypotonus with hypertonus of the limbs, he could not hold his head up. The electroencephalogram (EEG) did not show abnormalities. Ocular examination showed a mild hypermetropic astigmatism. Brain MRI was normal and a neurometabolic work-up did not show significant abnormalities. The last neurologic examination was performed at 5 years of age. The speech was absent and the child still showed axial hypotonus with no trunk control and inconstant head control. The inferior limbs were hyperextended with a dystonic posture. He could manipulate objects (with his left hand preferentially), but mobility is impaired by frequent dystonic-dyskinetic movements.

*Family 5: p.Y471**

Family 5 is Hispanic (Guatemalan) and the male fetus was identified prenatally with multiple brain abnormalities (Table S1). The mother is a 21-year-old G2P1000 whose first child died of Ebstein's anomaly shortly after birth. At 21 6/7 weeks, the affected male fetus showed absent bilateral mid- and posterior cerebral hemispheres, with no midline falx; cerebellum smaller than expected for gestational age; and enlarged cisterna magna thought to be secondary to the small cerebellum. On the follow-up ultrasound at 32 weeks, the head circumference was at the 98th percentile. Postnatal MRI showed a large posterior midline cystic structure, which likely represents a dilated left lateral ventricle related to obstructive hydrocephalus. There was a significant and progressive effect on the remaining cerebral hemispheric structures, brainstem, and cerebellum that had progressed from the prior fetal MRI. Additionally, there appeared to be underlying congenital brain anomalies with dysplastic/polymicrogyria changes involving the right cerebral hemisphere most notable in the right frontal region, as well as dysplastic changes involving the entire cerebellum. Furthermore, MRI showed congenital inner ear anomalies with dysplastic combined vestibule/lateral semicircular canals bilaterally. We enrolled the family in a fetal brain anomaly trio sequencing project, performed parent-proband genome sequencing and identified a maternally-inherited frameshift indel in *SRPK3*: (NM_014370.4): c.1413_1414del;

p.Y471*. The variant was absent from gnomAD and confirmed by Sanger sequencing in the proband (hemizygous) and mother (heterozygous). In addition, we found rare missense variants in 2 additional genes *BAALC* NM_024812.3: c.263C > A, p.P88Q (homozygous), *LOC400499* NM_001370704.1: c.9482A > C, p.K3161T and c.7209C > A, p.S2403R (compound heterozygous). Neither gene has been implicated in human genetic disease, and all variants are considered variants of uncertain significance (VUS).

Expression of SRPK3 *in the Central Nervous System of Human and Zebrafish*

Experiments confirmed the expression of *SRPK3* in the human fetal brain and heart. At Carnegie stage (CS) 15,[9] widespread *SRPK3* expression was observed within the developing brain, retina, spinal cord, heart muscle, and limbs. The expression predominantly occurred in post-mitotic cells and non-nuclear. At CS19, *SRPK3* expression was detected in the cerebellum and medulla, with particularly strong expression in the hindbrain choroid epithelium. Notably, at CS23, a robust expression was identified in the choroid epithelium, while comparatively weaker expression was observed in the cerebellum, pons, and medulla. In both stages, expression occurred mostly in post-mitotic cells, although both nuclear and cytoplasmic staining were seen (Fig 2A–C). Analysis of the RNA-Seq dataset revealed an age-dependent increase in *SRPK3* mRNA expression, with the highest levels noted within the cerebellum (Fig S2). To investigate the spatiotemporal expression patterns of *srpk3* during zebrafish development, WISH was performed. Robust expression of *srpk3* transcripts was detected at 24 hous postfertiliztion (hpf), with specific expression observed in the brain, heart, and muscle. By 72 hpf, the expression remained prominent in the brain and central neural tissues. Notably, distinct expression could be observed in the retinal layers of zebrafish larvae. Interestingly, both human and zebrafish embryos exhibited high levels of *SRPK3* expression in the developing retina (Fig 2C,D), implying a conserved role of *SRPK3* in eye function.

Molecular Modeling Reveals Structural Impacts of Missense Variants

We analyzed the effects of the 4 XLID-associated missense variants (H159D, S318L, T458N, and E529K) on *SRPK3* whose structure was modeled by Alphafold (https://alphafold.ebi.ac.uk/entry/Q9UPE1) (Fig 3A). We focused on the 3 variants H195D, T458N, and E529K. For S318L, as this variant occurs in the second unstructured loop region (residues 310–385), its effects were unable to be predicted by molecular modeling. We found that the H159D and T458N substitutions can cause protein misfolding, because His159 and Thr458 are located in the interior of *SRPK3* and their side chains play a structural role for the maintenance of the protein folding (Fig 3B). For instance, while the imidazole ring of His159 mediates 72 atom–atom contacts within the distance of 4.5 Å, the corresponding contacts mediated by the side chain carboxyl group decrease to 39 due to the H159D substitution (Fig 3B). Additionally, the T458N variant appears to cause steric hindrance with the neighboring bulky residues such as Phe454, Tyr528, and Trp530, presumably resulting in disturbance of *SRPK3* protein folding (Fig 3B). In contrast, the side chain of Glu529 is exposed to the outside of the protein, and thus its substitution to lysine seems not to affect protein stability. Instead, we noticed that *SRPK1* and *SRPK3* share a high structural similarity with each other with a root-mean-square deviation value of 0.73 Å over 343 aligned Cα atoms, and Glu529 is located adjacent to the SRPK1-bound protein fragment in the superposed model (Fig 3C). Therefore, we suppose that the E529K substitution leads to alteration of protein shape and surface charge, which finally affect the protein–protein interaction-mediated target protein recognition of *SRPK3* (Fig 3D).

New insights from molecular modeling of *SRPK3* variants led us to analyze the subcellular localization of *SRPK3* WT and variants. To examine the subcellular localization of *SRPK3* variants in cultured cells, we transfected GFP-tagged *SRPK3* WT and variants into HeLa cells, and GFP fluorescent image was examined under confocal microscope. Fluorescence cytochemistry revealed that *SRPK3* WT, S318L and E529K variants were mainly expressed in the nuclei, while the H159D and T458N variants exhibited cytosolic localization (Figs 3E and S9). These results imply that important roles of H159 and T458 in proper protein folding of *SRPK3*, as suggested by molecular modeling, contribute to the subcellular localization of *SRPK3*.

Generation of srpk3 *KO Zebrafish Lines Using CRISPR-Cas9 System*

Human *SRPK3* is located on Xq28, while the zebrafish *srpk3* homologue is located on chromosome 8. A ClustalX 2.1 alignment of their amino acid sequences revealed a high degree of conservation (Fig S3). The human homologue contains 567 amino acids, while the zebrafish homologue consists of 701 amino acids. The missense variants H159D, S318L, T458N, and E529K are marked with red arrows in Figure S3A. To investigate the functional consequences of *srpk3* mutations in zebrafish, we employed CRISPR-Cas9 technology to generate KO zebrafish lines. The specific target sites at the exon of *srpk3* were designed, and the

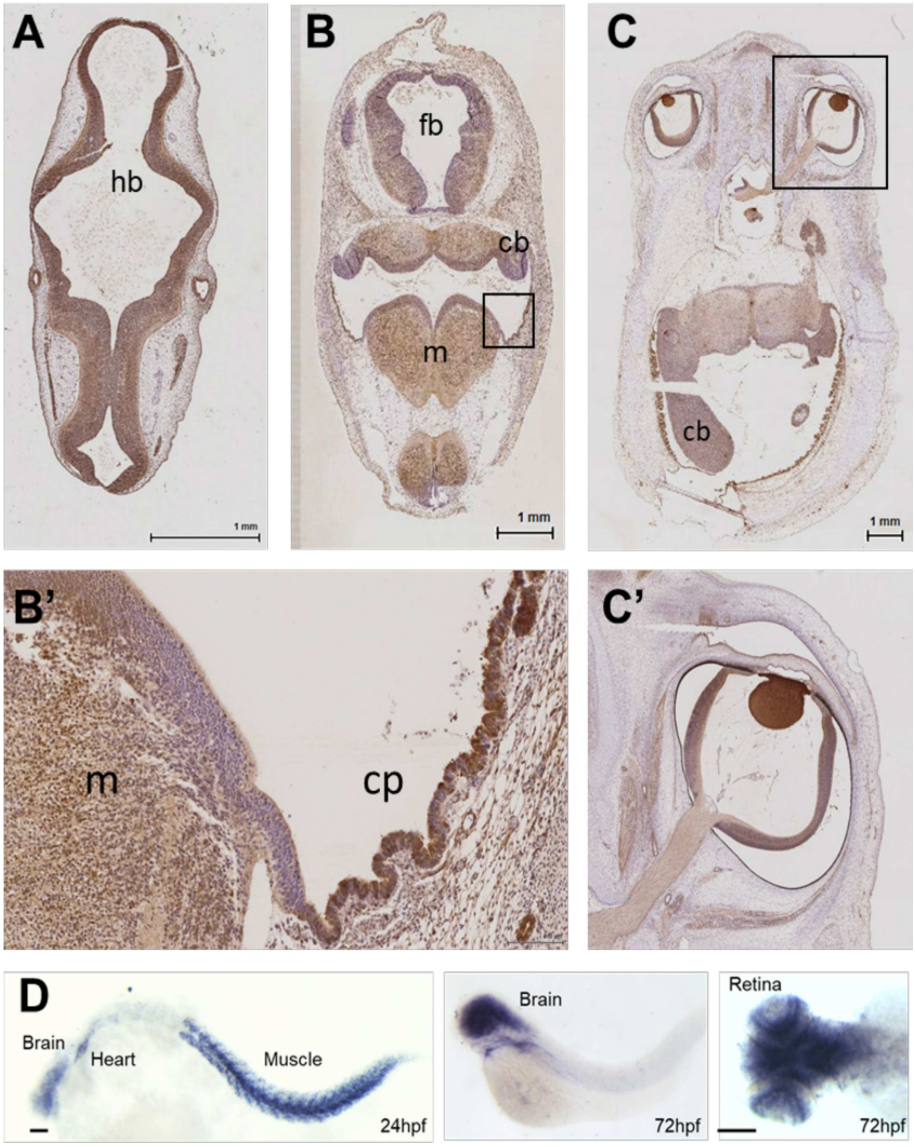

FIGURE 2: CNS expression of *SRPK3* in human and zebrafish embryos. (A) At Carnegie stage 15 (CS15), immunohistochemistry results showing widespread staining of *SRPK3* within the hindbrain (hb). (B) At CS19 postmitotic expression is noted in the forebrain (fb), cerebellum (cb) and medulla (m). (C) At CS23 expression is noted in cerebellum. (B′, C′) High magnification images showing intense staining of choroid plexus (cp) epithelium and expression within the cerebellum (cb), medulla (m), and eye. (D) Spatiotemporal expression of *srpk3* in developing zebrafish embryo showing transcripts of *srpk3* being present at 24 hpf in the brain, heart, and muscles, and in the brain and retinal layers at 72 hpf. Scale bars: 1 mm for (A–C), 100 μm for (D).

induced mutations were analyzed by sequencing. The resulting KO mutant forms included +27, +1, −3, −8, −4, and −7 bp (Fig S3B). For our experiments, we utilized a *srpk3* KO zebrafish line harboring an in/del mutation predicted to produce truncated proteins (Fig 4A).

Swim Bladder Defects in srpk3 *KO Zebrafish at Early Developmental Stage*

The *srpk3* KO zebrafish exhibited normal development during early embryonic stages. Assessment of cell death using acridine orange staining, a marker of apoptotic cells in zebrafish, showed no significant differences compared to WT (Fig S5). Subsequent analysis focused on morphological defects in larval zebrafish at 5 dpf, including body length, pigment patterns, and eye size. No significant abnormalities were observed in these aspects. However, a notable finding was that the majority of KO zebrafish had defective swim bladder inflation, a crucial early marker of survival in larval zebrafish as it enables them to swim (Fig 4B). A total of 2,367 larvae from 10 independent clutches were examined, and the incidence of swim bladder defects was decreased from 23.4 to 4.3% in subsequent generations (Table S2). Notably, only 6 out of 73 (8%) *srpk3* KO zebrafish survived

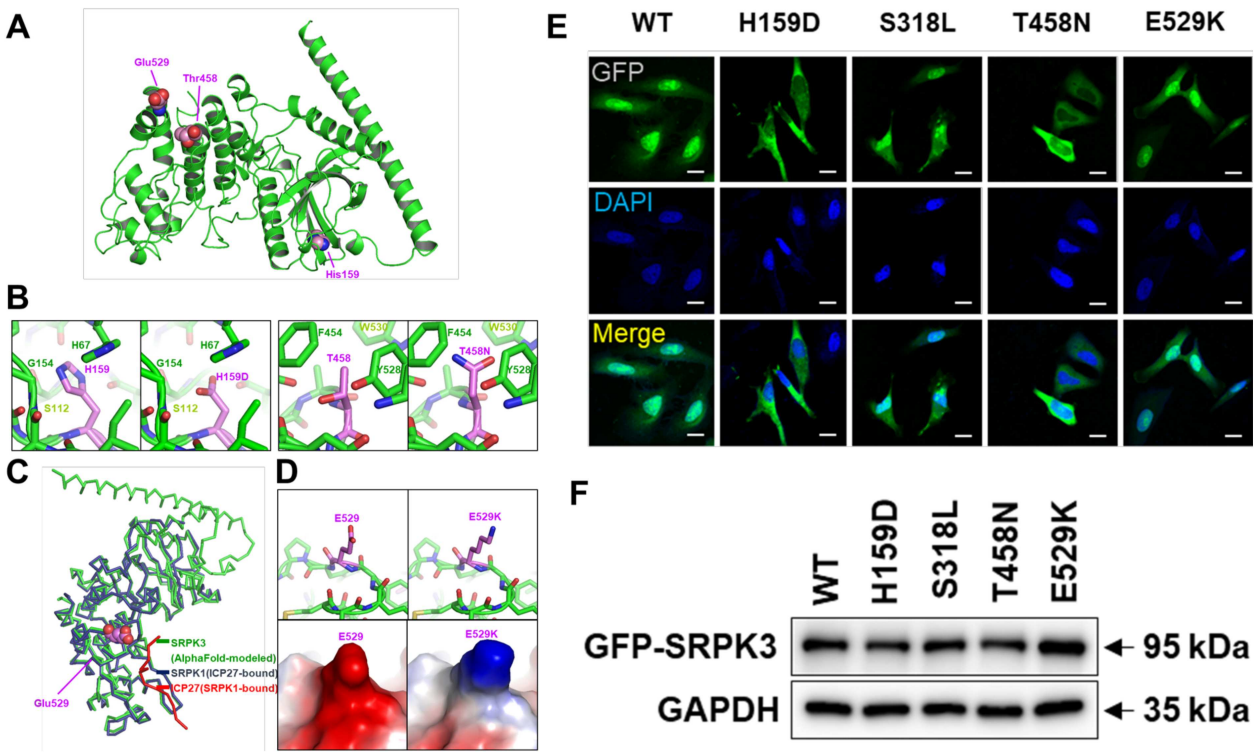

FIGURE 3: Molecular modeling of *SRPK3* and subcellular localization of *SRPK3* variants in HeLa cells. (A) Side chains of 3 amino acids involved in X-linked intellectual disability (XLID) are indicated as spheres on the *SRPK3* structure modeled using AlphaFold. Unstructured loop regions of *SRKP3* are omitted for clarity, including residues 1–46 and 310–385. (B) Interior misfolding due to H159D and T458N variations. *SRPK3* wild-type (WT) left and the H159 and T458N variant form modeled based the AlphaFold structure prediction are shown together. (C) Structural superposition of the AlphaFold-modeled *SRPK3* (green) onto the crystal structure of ICP27 (red)-bound SRPK1 (Navy; PDB code 6FAD). Side chain atoms of *SRPK3* Glu529 are presented as spheres. (D) Alteration of protein shape and surface charge due to E529K variation. *SRPK3* WT (left) and the E529K variant form (right) are shown as sticks and loops (top) or electrostatic surface representation (bottom). (E) Fluorescence cytochemistry images were obtained to compare the localization of *SRPK3* WT and variants. Cell nuclei were stained with DAPI, and localization of *GFP-SRPK3* was analyzed by observing GFP fluorescence using confocal microscopy. Scale bars; 20 µm. (F) Western blot analysis of *GFP-SRPK3* was conducted to confirm the transfection efficiency of WT and variant plasmids. GAPDH served as a loading control.

into adulthood (Fig S4). This highlighted the lack of swim bladder inflation as a significant feature which prompted further molecular marker analysis.

Next, we performed overexpression studies in *srpk3* KO zebrafish larvae. We aimed to validate the effects of WT and variant forms of *SRPK3* in *srpk3* KO zebrafish, using swim bladder inflation as the criterion for functional studies. Initially, we injected 200 pg of WT *SRPK3* mRNA into 1-cell stage zebrafish embryo. However, we did not observe any swim bladder inflation in *srpk3* KO zebrafish. Subsequently, we increased the concentration to 500 pg yet swim bladder inflation remained elusive. Despite this, we opted to inject 500 pg of H195D *SRPK3* mRNA, but there were not significant changes observed in the phenotype (Fig S6A). Additionally, we did not observe significant morphological changes after overexpression of S318L *SRPK3* variant in WT zebrafish (Fig S6B). Taken together, we concluded that since swim bladder inflation only happens at relatively later stage of development where stability of mRNA at that stage could be a reason because effects of mRNA being transient.

Expression of Neuronal or Muscle Markers in srpk3 *KO Zebrafish*

The mRNA expression levels of early neurogenesis marker *her4* was examined in WT and KO *srpk3* zebrafish siblings using WISH. No significant changes were observed in the expression of these molecular markers in the homozygous KO zebrafish compared to the WT. Similarly, the analysis of the motoneuron marker *islet 1* and the dopaminergic neuronal marker *tyrosine hydroxylase* (*th*) in KO zebrafish did not reveal significant differences compared to its WT siblings (Fig 4C). Furthermore, the expression of other neural markers (*phox2b*, *ascl1*, *dlx2*), a cell cycle marker (*ccdn1*), and muscle markers, *bridging integrator 1b* (*bin1b*), and *tandem duplicate 1* (*ttnb*) showed no significant differences between KO and WT siblings at early developmental stages (Fig S7). However, overall expression of *srpk3* transcripts were decreased in KO zebrafish

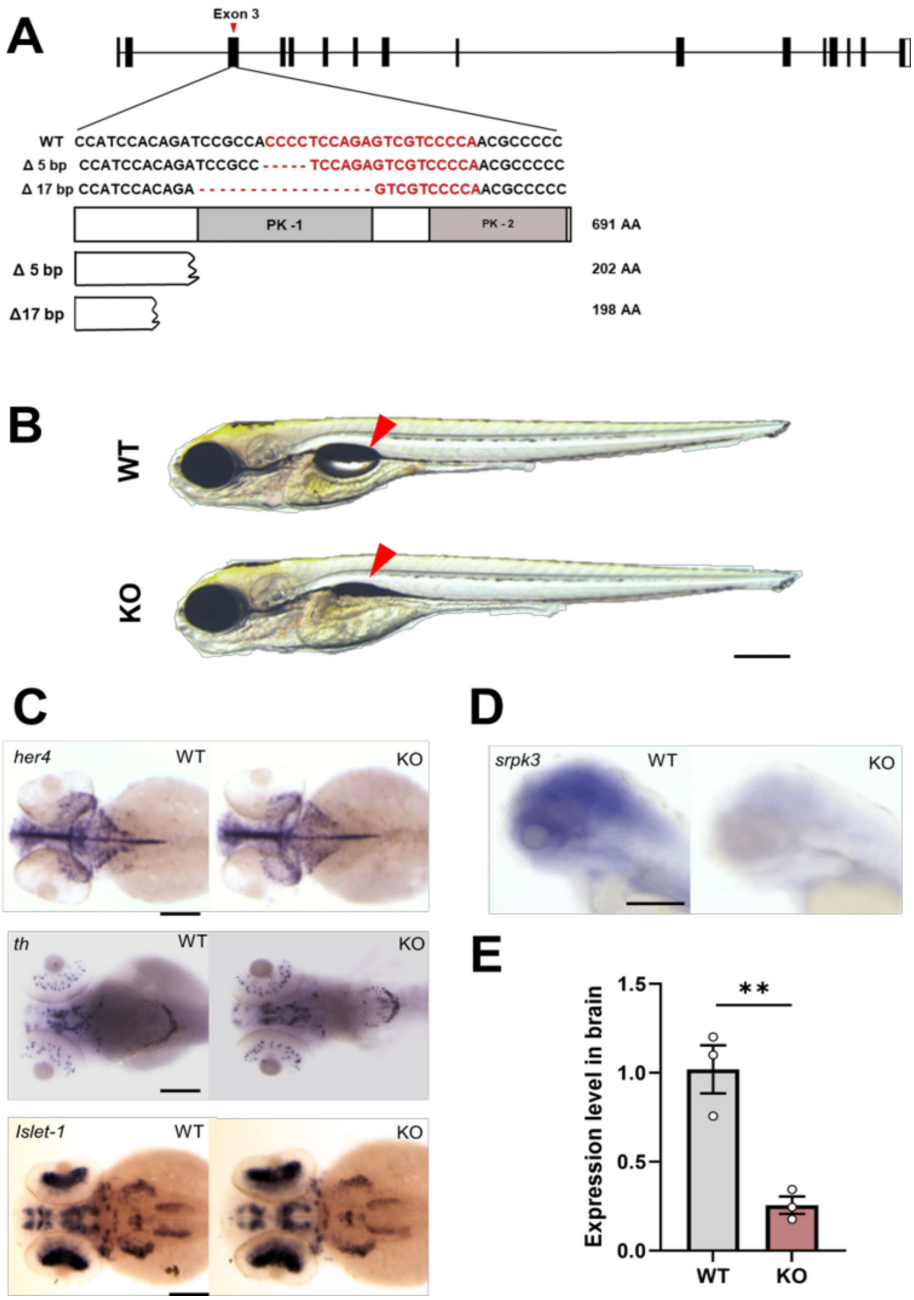

FIGURE 4: Generation of *srpk3* zebrafish knockout (KO) line. (A) Disruption of protein domains in KO zebrafish while wild-type (WT) zebrafish show intact *srpk3* protein. Protein kinase domain 1, PK-1; protein kinase domain 2, PK-2. (B) KO zebrafish fail to develop swim bladder inflation at 5 dpf when compared to WT siblings (red arrow). (C) Expression analysis of neuronal markers (*her4*, *th*, *islet1*) and *srpk3* at 72hpf. Scale bars; 200 µm. (D, E) Reduced expression level of *srpk3* mRNA in KO zebrafish. Three adult brains for each group were used in qRT-PCR experiments ($n = 3$ for WT and $n = 3$ for KO).

indicating nonsense-mediated decay in KO zebrafish (Fig 4D). *srpk3* mRNA expression level in adult brain was also confirmed by qRT-PCR (Fig 4E). Three adult brains were used for each qRT-PCR experiment.

The srpk3 *KO Zebrafish Show Defects in Spontaneous Eye Movements*

Neurodevelopmental disorders are sometimes associated with specific eye abnormalities such as ocular motor apraxia and nystagmus. Spontaneous eye movements in vertebrates follow a distinct pattern of saccades in 1 direction, fixation, and then a saccade in the opposite direction.[18] To investigate the role of *srpk3* in ocular anomalies, we examined spontaneous eye movements in 5 dpf zebrafish larvae. In WT *srpk3* siblings, both eyes moved synchronously in a unidirectional pattern,[19] crucial for maintaining spatial connection in the visual spectrum.[20] However, *srpk3* KO siblings exhibited a significant reduction in eye movement frequency (Fig 5A, B); indicating

a role of *srpk3* in maintaining the movement pattern. Although most WTs displayed robust synchronized movements in both eyes, KO zebrafish also showed a reduction in eye movement frequency (Fig 5C), ocular angle (Fig 5D), and reset time (Fig 5E), suggesting disruptions in eye coordination. However, KO zebrafish exhibited normal color response at 5 dpf (Fig S8) in a color preference test, which we had previously developed.[21] These findings suggest that *srpk3* KO zebrafish have significant impairments in spontaneous eye movement, potentially contributing to syndromic intellectual and learning disabilities.[22-24]

Eye movement defects have been reported in other neurological disease models in zebrafish, such as down syndrome cell adhesion molecule-like 1 (*dscaml1*), which is thought to be involved in autism spectrum disorder (ASD) and cortical abnormalities. These defects manifested in behavior resembling congenital ocular motor apraxia.[25] Similarly, the KO zebrafish models of *taf1*[26] and *katnal2*,[27] genes associated with intellectual disability, exhibited notable eye defects. Additionally, zebrafish *belladonna*/(*lhx2*) mutants demonstrated significant contributions to congenital nystagmus[28,29] and agenesis of the corpus callosum, as observed in *Lhx2* mutant mice.[30]

Impaired Social Interaction in srpk3 *KO Zebrafish*

We previously established a behavioral assay in zebrafish[17] to assess social interaction. Impaired social interaction is 1 of the primary indicators of intellectual disability in humans. Given that social interaction-affecting abnormalities were also observed in the affected patients (Table S1), we conducted social interaction testing on *srpk3* KO zebrafish (Fig 6). To quantify social interaction in zebrafish, we divided the tank into 4 zones (1, 2, 3, and 4) and measured the time the single experimental fish (either *srpk3* KO or WT sibling) spent in each of these zones (zone 1 closest and zone 4 furthest away from the stimulus fish) (Fig 6A). Our results demonstrated that overall WT siblings stayed in zone 1 (closest to the stimulus fish) and appeared to frequently interact with the stimulus fish. In contrast, *srpk3* KO zebrafish stayed in zone 1 for significantly shorter time and instead explored the entire tank, including zones 2, 3, and 4 (Fig 6B). The difference between control and KO fish was particularly robust at the early phase of the behavioral session as *srpk3* KO adult zebrafish displayed impairments in their response to social stimuli (sight of conspecifics), during the minutes 1–6. When we analyzed the behavior of the fish at 2 time intervals: the early phase (2–7 min) and the late phase (10–15 min) of the session (Fig 6C), we found that during the early phase, control WT fish remained in zone 1, close to the social cue, indicating that the control test fish could perceive the visual stimuli, and could appropriately respond to them. But, *srpk3* KO test fish tended to move around the tank and interacted much less with the stimulus fish. However, in the late phase, both *srpk3* KO and WT fish interacted more the stimulus fish as well as exploring the environment of the tank. Combined together, the above findings imply unimpaired general locomotory abilities, unimpaired exploratory behavior, but impaired shoaling (social) response in the KO mutant fish compared to control counterparts.

Subsequently, we have performed shoaling bowl assay to further validate impaired social interaction in *srpk3* KO zebrafish. Zebrafish form shoals, in which individuals swim close to each other, a behavior observed in nature and one which can be easily quantified in the test tank as social or shoal cohesion.[17] The distance between individual fish is used to determine the social cohesion (Fig 6D). We have used a flat bottom round bowl (Fig 6E, F) to investigate shoaling behavior in zebrafish. We have used 3 siblings from each genotype per trial. WT zebrafish appeared to interact with each other throughout the test keeping the inter-individual distance between the fish relatively low. In contrast, *srpk3* KO zebrafish did not appear to interact with one another and exhibited decreased shoal cohesion, ie, increased inter-individual distance (Fig 6G). These findings again demonstrate impaired shoaling response in *srpk3* KO zebrafish compared to their WT siblings.

What may be the neurobiological bases of this impairment in social behavior? Because we did not detect significant changes in the expression of the 2 neuronal makers we examined during early developmental stages of control and KO fish, we decided to conduct further analysis of the adult brain, including analysis of potential anatomical defects, the topic of the subsequent section of this paper.

Reduced Valvular Cerebelli in Adult srpk3 *KO Zebrafish*

Although impaired social interaction was observed in adult *srpk3* KO zebrafish, we did not find a significant difference in growth and body size between WT and *srpk3* KO siblings, indicating that general health and ability to move and capture food have not been affected by the mutation in the KO fish. Next, we investigated the potential impact of the *srpk3* null mutation on brain size, considering our previous findings of reduced brain size associated with behavioral deficits seen in a zebrafish autism model.[17] We examined adult whole brains, and observed no significant difference in overall size between WT and *srpk3* KO siblings (Fig 7A, B). Subsequently, we performed brain sectioning at a thickness of 7 μm in both WT and KO zebrafish, followed by H&E staining to analyze neuroanatomical structures in detail. We noticed a remarkable reduction in a specific brain region

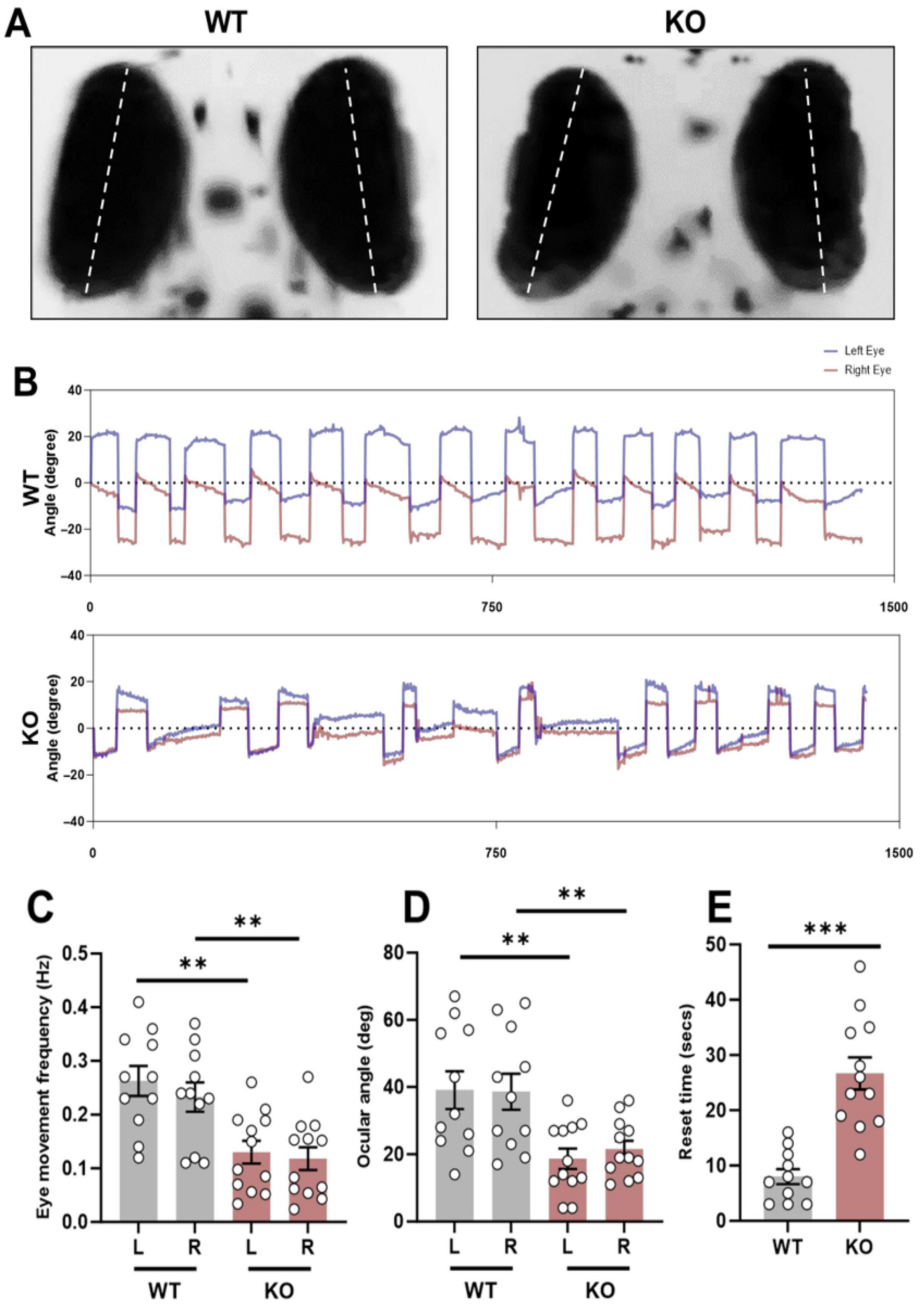

FIGURE 5: Analysis of spontaneous eye movements in knockout (KO) zebrafish. (A) Representative image of spontaneous eye movement in wild-type (WT) and KO zebrafish at 5 dpf. (B) Individual representation of spontaneous eye movement in WT and *srpk3* KO siblings. Red lines represent right eye and blue lines represent left eye of 5 dpf zebrafish larvae. (C) Eye movement frequency in the left (L) and right (R) eye of *srpk3* KO zebrafish when compared to its WT siblings. (D) Ocular angle significantly decreases in both left and right eye in KO zebrafish, compared to WT siblings. (E) *srpk3* KO zebrafish take significant longer time to reset in slow phase when compared to their WT siblings during spontaneous eye movement. Video recording of WT ($n = 11$) and KO ($n = 12$) zebrafish for 3 min. All data is represented as mean ± SEM. **$p < 0.01$, ***$p < 0.001$ by *t* test.

known as the valvular cerebelli in the KO fish (Fig 7C, D). The relative size of valvular cerebelli of *srpk3* KO zebrafish and their WT siblings was measured by ImageJ analysis of the area of valvular cerebelli (Va) region divided by the total area of the brain in the slice. Va% = Size of Va / size of total brain X100. We observed that the relative size of valvular cerebelli in the whole brain of *srpk3* KO zebrafish was reduced to 50%, 59%, and 41% compared to that of WT zebrafish in 3 different sections (Fig 7C–E). a significant change suggesting a potential role of *srpk3* in the development and maintenance of this specific brain region.

Discussion

In this study, we provide multiple lines of evidence for the role of *SRPK3* in neurodevelopment and XLID. We

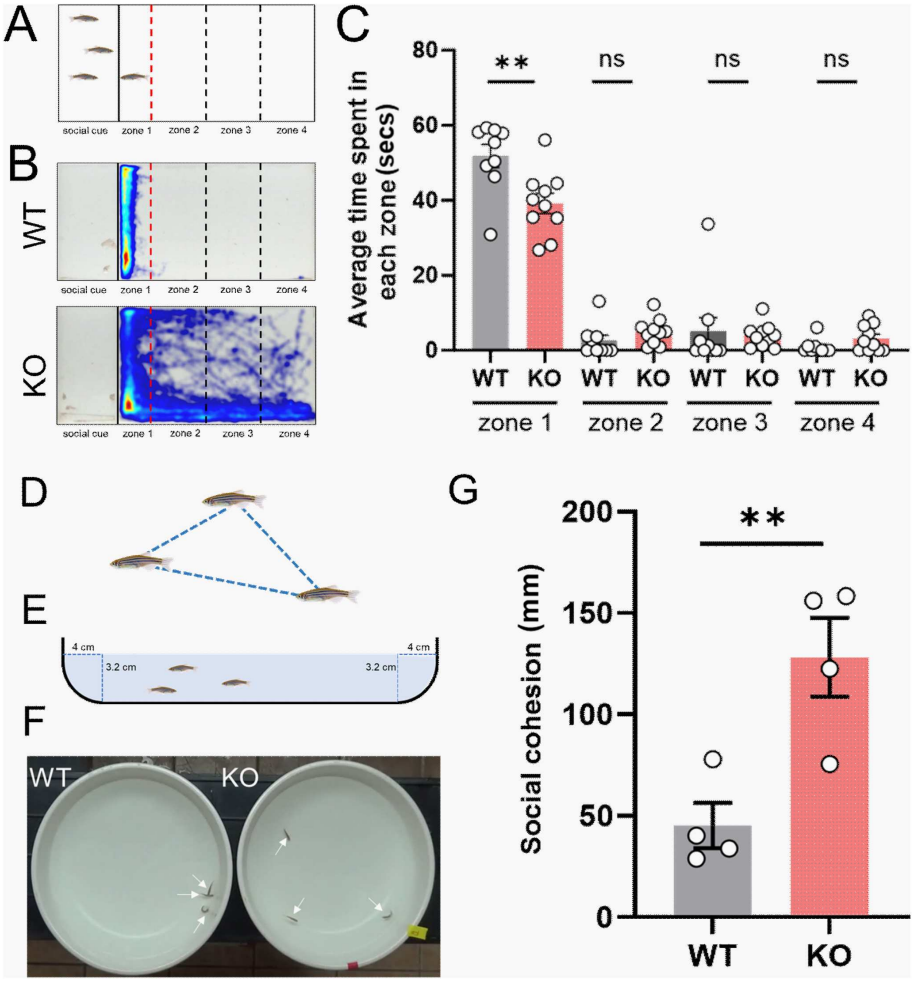

FIGURE 6: ***srpk3*** **knockout (KO) adult zebrafish show impairment in social interaction. (A) Representative image of the experimental setup of social interaction assay in adult zebrafish. (B) Heat map analysis of social interaction assay in adult zebrafish. Three wild-type (WT) fish were used as social cue and 1 as an experimental fish. Black bold line indicates the position of the transparent separator in the water tank. Red and black dashed lines show relative positions of 4 different zones. Video tracking was analyzed at 2 different time bins; early stage (2–7 min) and late stage (10–15 min), respectively. (C) Mean time spent by the experimental fish in each zone at late stage of social interaction assay. (D) Representative image of 3 shoaling fish. (E) Representative image of the parameters of bowl used for shoaling bowl assay. (F) Experimental set up for shoaling bowl assay. Individual adult fish were pointed by arrows. (G) Quantified data for the average of the inter-fish distance of the shoaling assay. The test was performed in triplicates. For each trial, 3 fish of each genotype were used. Number of experimental fish used;** $n = 10$ **for WT and** $n = 10$ **for KO. All data are represented as mean ± SEM. **** $p<0.01$ **by** *t* **test.**

identified novel *SRPK3* variants that segregated with the phenotype in 5 unrelated families. Using artificial intelligence (AI)-based structural protein modeling and subcellular localization experiments, we elucidated the impact of these missense variants on *SRPK3*'s structure and their potential role to disrupt normal *SRPK3* functioning. Moreover, we provided novel insights into the early expression patterns of *SRPK3* in human embryonic and fetal brains, demonstrating a correlation between *SRPK3* expression and the observed brain phenotypes in our patients using neuroimaging techniques. This is the first report of such expression patterns for *SRPK3*. To further validate the role of *SRPK3* in XLID, we employed histological analysis, social interaction assays, and oculomotor behavior assay in a novel *srpk3* zebrafish KO model. These experiments successfully recapitulated some of the human phenotypical abnormalities, establishing the relevance of *SRPK3* in the pathogenesis of XLID.

One critical cellular activity essential for gene expression and the generation of multiple protein isoforms from a single pre-mRNA molecule is the processing of pre-mRNAs by the spliceosome, a complex comprising many components.[31] SR proteins, a family of proteins containing an arginine/serine-rich (RS) domain, play a crucial role in spliceosome function.[32] However, phosphorylation of SR proteins by SR protein-specific kinases (SRPKs) is necessary for their functionality.[7] *Srpk3* is primarily expressed in the heart and skeletal muscles of mice,

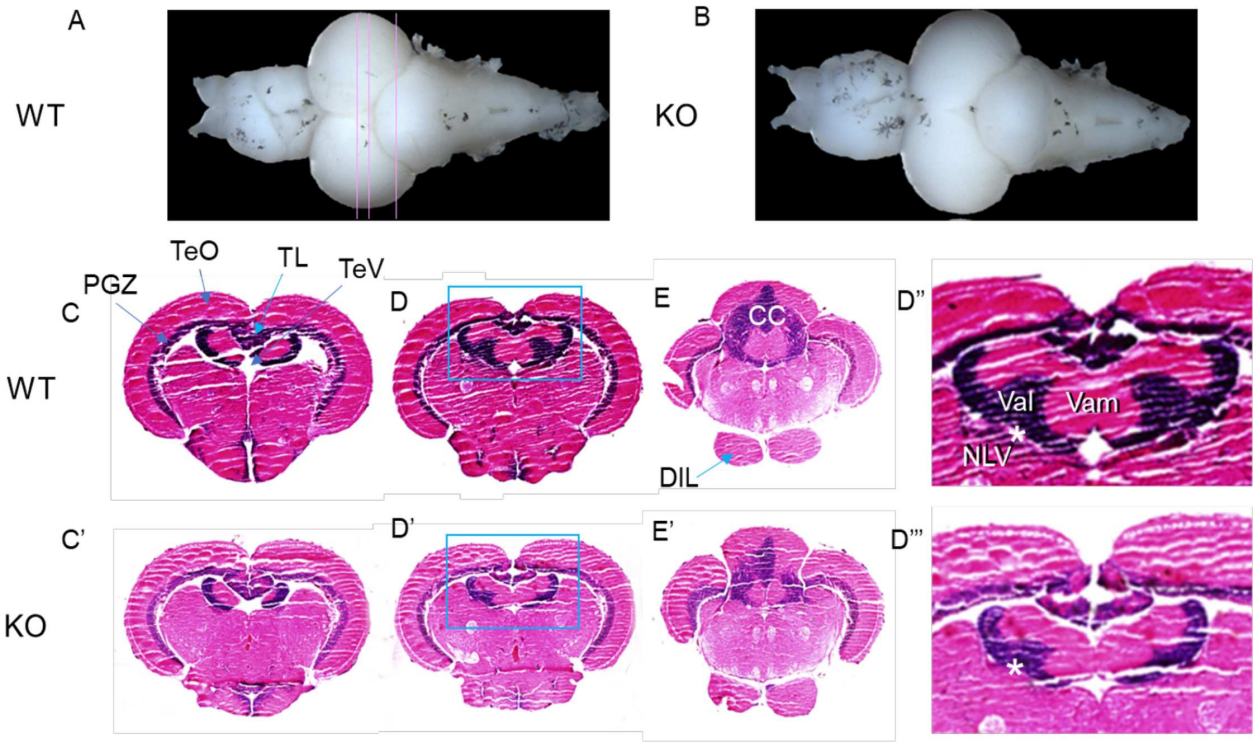

FIGURE 7: Reduced size of the valvular cerebelli in adult brain of *srpk3* KO zebrafish. (A, B) Representative whole brains dissected from a control wild-type (WT) and a knockout (KO) zebrafish. Doral view, anterior is to the left. (C, D‴) Anatomical analysis of brain sections after H&E stain. Frontal sections at 3 different levels indicated in (A). (D″–D‴) Enlargement of valvular cerebelli region in the inlets in (D) and (D′). Asterisk indicates a structural connection between the nucleus lateralis valvulae (NLV) and the valvular cerebelli. Number of adult zebrafish brain used for analysis; $n = 3$ for WT and $n = 3$ for KO. CC = corpus cerebelli; DIL = diffuse nucleus of the inferior lobe; NLV = nucleus lateralis valvulae; PGZ = periventricular gray zone of optic tectum; TeO = tectum opticum; TeV = tectal ventricle; TL = torus longitudinalis; Val = lateral division of valvular cerebelli; Vam = medial division of valvular cerebelli.

suggesting its involvement in muscle development. A study of *Srpk3* KO mouse reported the presence of myopathy.[33] However, it is important to mention that in a high-throughput myopathy phenotype screening of over 4,000 KO mice, myopathy was not detected.[34] Notably, in our study, *srpk3* KO zebrafish did not exhibit any signs of myopathy (Fig S5). However, recently, a new function of SRPK2 was reported in synaptic vesicle function and neurotransmitter release.[7] In addition, association of *Srpk3* protein expression was described in a mouse model of Parkinson's disease.[35]

Since SRPKs have not been well characterized, the identification of pathogenic missense variants in *SRPK3* represents a significant discovery. The first variant (H159D) was located in the first protein kinase domain, while the second (T458N) and third (E529K) variants were found in the second protein kinase domain, suggesting potential effects of these variants on kinase mediated SRPK protein function. Although, further studies with phosphorylation assays are required to confirm this prediction, molecular modeling using Alphafold demonstrated that the H159D and T458N variants led to protein misfolding, while the E529K variant could affect protein–protein interaction. Supporting this prediction, subcellular localization experiments revealed that *SRPK3* WT, S318L and E529K variants were mainly expressed in the nuclei, while the H159D and T458N variants exhibited cytosolic localization. Thus, SPRK3 S318L and E529K may be hypomorphic alleles. We also note that, although rare, the p.E529K variant is reported in 32 males in the gnomAD database (v.4.0.0). It is possible that this variant has incomplete penetrance and/or that it exerts its effect only on a specific genetic background. Additional assays will be needed to determine the precise impact of the missense variants on SPRK3 function.

Swim Bladder Defects in Zebrafish Models of Neural Diseases

The swim bladder serves as an air-filled organ important for maintaining neutral buoyancy in numerous fish species. Primary inflation of the swim bladder by surface air gulping is a critical developmental milestone required for independent swimming and survival.[36] In zebrafish, there exists a critical timeframe within which primary inflation must occur

by capturing a small gas bubble from the water's surface. This process, known as "swim-up behavior," involves repetitive upward movements toward the water surface, and encompasses a complex integration of multiple physiological systems, including gravity sensing, motor development, neurological function, and/or visual acuity.[37] In our previous studies, we observed swim bladder defects in several zebrafish KO models of neurodevelopmental disorders, including XLID with spasticity,[38] Armfield XLID syndrome,[39] and ataxia,[40] suggesting that the swim bladder defect may be classified as a neurodevelopmental disorder.

Eye Movements and Intellectual Disability

Visual attention and perception are influenced by 2 key functions of the eye: fixation and tracking. Fixation is the act of precisely positioning the target object onto the fovea, while tracking refers to the ability to maintain focus on moving objects. Impaired eye movements have been associated with learning difficulties and intellectual disability.[22-24] Convergence insufficiency is characterized by a decreased ability to converge the eyes and maintain binocular fusion while focusing on a nearby target. On the other hand, smooth pursuit refers to the ability of the eyes to slowly follow a moving target. It is frequently observed that children with learning disabilities have an underdeveloped function of smooth pursuit. Advancements in eye tracking technologies have enabled more sophisticated methods for studying eye movement. For instance, dyslexic children have exhibited poor pursuit performance with increased catchup saccades and decreased gain values.[41] Eye movement studies in individuals with schizophrenia have revealed cognitive dysfunction, and a genetic link between physiological characteristics and smooth pursuit eye movements.[22,23] Similarly, high functioning individuals with autism have demonstrated deficits in eye movements compared to their neurotypical peers of the same age group.[42] These findings demonstrate the association between eye movement abnormalities and intellectual disabilities, although, notably, the direction of causality in the association is not always clear.

Oculomotor Behavior and Neural Circuit Function

Loss of *srpk3* resulted in a notable impairment in oculomotor behavior, particularly evident in the frequency of spontaneous eye movements and the reset time following eye movement, as observed in *srpk3* KO zebrafish compared to controls. These oculomotor behaviors observed in KO zebrafish may arise in part from a deficit in the circuit connectivity within the integrator, a key component for supporting and coordinating persistent firing.[43,44] The delayed reset time in KO zebrafish may partly arise from defects in the integrator pathway, which is essential for controlling a smooth ramp of eye position.[45]

The human eye contains 6 extraocular muscles that are responsible for controlling eye movements. These muscles include the superior rectus, inferior rectus, medial rectus, lateral rectus, superior oblique, and inferior oblique muscles. Each of these muscles plays a specific role in moving the eye in different directions. The precise coordination of these neuromuscular activities allows for smooth and precise eye movements. To examine structural defects in extraocular muscles in *srpk3* KO zebrafish, we introduced muscle markers, *bridging integrator 1b* (*bin1b*), and *tandem duplicate 1* (*ttnb*), and found no significant change at least in gene expression level (Fig S6).

Oculomotor anomalies can arise from impairments in the eye muscles responsible for controlling eye movements, further contributing to the complexity of eye movement disturbances in certain cases. However, the genetic factors underlying eye movement are largely unknown. Recent genetic studies examining eye movement phenotypes have predominantly focused on identifying mutations in candidate genes associated with the risk of schizophrenia.[46] Given the lack of our understanding of how genetic factors contribute to eye movement impairment and whether eye-movement abnormalities seen in neurological disorders are due to central nervous system (CNS) dysfunction or eye muscle-related problems, one must consider both neuronal and muscle function-related mechanisms in future studies of SRPK function.

Reduction in the Size of Valvular Cerebelli in KO Zebrafish

Retinal projections in vertebrates exhibit topographical organization within the optic tectum (known as the superior colliculus in mammals). Somatosensory impulses from the optic tectum are conveyed to the cerebellum, a vital structure involved in motor control, cognition and emotion. In fish, the cerebellum consists of the valvula cerebelli, corpus cerebelli and caudoventral cerebellar regions. The nucleus lateralis valvulae (NLV), a cerebellar relay nucleus, is functionally similar to the pontine nuclei in mammals.[47] Thus, the retino-pretectal-NLV-valvular-cerebellar corpus pathway likely plays a role in visual and somatosensory information processing. In this study, we observed a reduction in the size of the valvula cerebelli, NLV and their connection in *srpk3* KO zebrafish. Although there are structural differences between the human and fish brain, many such structures have been shown to have conserved roles.[48,49] Recent studies have provided molecular insights into the new role for the cerebellum in cognitive behaviors, including its function in the modulation of dopaminergic

reward circuits, language and social behavior. They have also identified a conserved cell type set that forms an archetypal cerebellar nucleus, representing the unit of cerebellar nuclei organization.[50] In zebrafish, the valvular cerebelli is suggested to serve non-locomotor functions, distinguishing it from the corpus cerebelli, which primarily contributes to locomotion.[51] Recently, we also observed a reduction of the valvular cerebelli size in other zebrafish models of neurodevelopmental disorders.[17,52] Therefore, future studies that selectively examine valvular cerebelli activity will provide further insights into the region- and class-specific roles of non-locomotory information processing within the cerebellar circuitry.

In patients, neuroimaging data revealed agenesis of the corpus callosum and colpocephaly. The corpus callosum, also known as the callosal commissure, is a wide and thick nerve tract found exclusively in placental mammals, absent in other vertebrates, including fish. Agenesis of the corpus callosum is a rare congenital disorder and 1 of the most commonly observed brain malformations in humans.

Individuals with colpocephaly experience varying degrees of motor disabilities, visual defects, spasticity, and moderate to severe intellectual disability. Colpocephaly often occurs as a result of hydrocephalus, the accumulation of cerebrospinal fluid (CSF) in the ventricles of the brain. Dilated ventricles, including colpocephaly, are frequently seen in individuals with agenesis of the corpus callosum. The precise reason for this phenomenon remains unclear, but the enlarged ventricles can be partially explained by reduced brain mass resulting from the agenesis of the corpus callosum. The exact causes for ventricular dilatation in agenesis of the corpus callosum are still subject to debate.[53] Obstruction of CSF pathways is absent, and hydrocephalus in these cases typically does not involve increased intracranial pressure. The choroid plexus (CP), a highly vascularized brain structure responsible for CSF synthesis, secretion, and circulation, has received increasing attention in recent years due to its association with neurodevelopmental and neuropsychiatric disorders.[54] Given that *SRPK3* is highly expressed in the CP epithelium, it would be intriguing to explore the potential involvement of *SRPK3* in CP development and function in future studies.

Acknowledgments

We express our gratitude to the participating families, with special appreciation to the members of Family 1, who have been involved in this study since 1984. This work was supported by grants from the National Research Foundation of Korea (2020R1A5A8017671 and RS-2024-00349650 to C.-H.K.), Ministry of Oceans and Fisheries (20220027), National Institute of Neurological Disorders and Stroke (NINDS) (R01NS073854 to C.E.S.), National Institute of Child Health and Development (NICHD) (R01HD105868 to N.L.V. and E.E.D.) and National Institute of Mental Health (NIMH) (R01MH106826 to E.E.D.), Ulverscroft Foundation and the South Carolina Department of Disabilities and Special Needs (SCDDSN) (2015-45 to C.E.S.), Ministero Italiano della Salute, Programma di Ricerca Finalizzata 2018 (Project ID RF-2018-12366314). M.G.T. is supported by the National Institute for Health Research (CL-2017-11-003) and Academy of Medical Sciences (SGL021/1066). R.G. is supported by NSERC (#311637). E.E.D is the Ann Marie and Francis Klocke, MD Research Scholar. Dedicated to the memory of Ethan Francis Schwartz, 1996–1998.

Author Contributions

C.H.K. and C.E.S. contributed to the conception and design of the study; M.G.T., C.S., G.M., M.C., H.H., C.S.C., T.W., B.N.C., M.F.H., I.G., A.E.C., C.G., T.P., E.I., F.M., G.S., C.T., C.F.B., T.N.K., K.G., H.Y., N.V., A.R., Y.R.L., T.I.C., T.Y.K., K.H.L., J.J.K., W.H.J.N., R.G., H.S.C., C.Y.C., S.K., J.H.Y., and B.K. contributed to the acquisition and analysis of data; A.R., C.H.K., C.E.S., H.G.K., R.G., E.E.D., M.G.T., and A.E.C. contributed to drafting the text or preparing the figures.

Potential Conflicts of Interest

The authors declare no conflict of interest.

Data Availability

Data supporting the findings of this study are available upon request from the corresponding authors.

References

1. Maulik PK, Mascarenhas MN, Mathers CD, et al. Prevalence of intellectual disability: a meta-analysis of population-based studies. Res Dev Disabil 2011;32:419–436.
2. Morton NE, Rao DC, Lang-Brown HE, et al. Colchester revisited: a genetic study of mental defect. J Med Genet 1977;14:1–9.
3. Neri G, Schwartz CE, Lubs HA, Stevenson RE. X-linked intellectual disability update 2017. Am J Med Genet A 2018;176:1375–1388.
4. Jansen S, Vissers LE, de Vries BB. The genetics of intellectual disability. Brain Sci 2023;13:231.
5. Tarpey PS, Smith R, Pleasance E, et al. A systematic, large-scale resequencing screen of X-chromosome coding exons in mental retardation. Nat Genet 2009;41:535–543.
6. Ghosh G, Adams JA. Phosphorylation mechanism and structure of serine-arginine protein kinases. FEBS J 2011;278:587–597.
7. Müller JA, Betzin J, Santos-Tejedor J, et al. A presynaptic phosphosignaling hub for lasting homeostatic plasticity. Cell Rep 2022;39:110696.
8. Desai J, Velo MP, Yamada K, et al. Spatiotemporal expression pattern of KIF21A during normal embryonic development and in

congenital fibrosis of the extraocular muscles type 1 (CFEOM1). Gene Expr Patterns 2012;12:180–188.

9. Bullen P, Wilson DI. The Carnegie staging of human embryos: a practical guide. In: Strachan T, Wilson DI, Lindsay S, eds. Molecular genetics of early human development. Oxford, 1997: 27–35.
10. O'rahilly R, Müller F. Developmental stages in human embryos: revised and new measurements. Cells Tissues Organs 2010;192: 73–84.
11. Miller JA, Ding SL, Sunkin SM, et al. Transcriptional landscape of the prenatal human brain. Nature 2014;508:199–206.
12. Hawrylycz MJ, Lein ES, Guillozet-Bongaarts AL, et al. An anatomically comprehensive atlas of the adult human brain transcriptome. Nature 2012;489:391–399.
13. Thisse B, Heyer V, Lux A, et al. Spatial and temporal expression of the zebrafish genome by large-scale in situ hybridization screening. Methods in cell biology 2004;77:505-519.
14. Vejnar CE, Moreno-Mateos MA, Cifuentes D, et al. Optimized CRISPR–Cas9 system for genome editing in zebrafish. Cold Spring Harb Protoc 2016;2016:pdb.prot086850.
15. Niederriter AR, Davis EE, Golzio C, et al. In vivo modeling of the morbid human genome using *Danio rerio*. J Vis Exp 2013;78: e50338.
16. Scheetz SD, Shao E, Zhou Y, et al. An open-source method to analyze optokinetic reflex responses in larval zebrafish. J Neurosci Methods 2018;293:329–337.
17. Kim OH, Cho HJ, Han E, et al. Zebrafish knockout of down syndrome gene, DYRK1A, shows social impairments relevant to autism. Mol Autism 2017;8:1–4.
18. Perez-Schuster V, Kulkarni A, Nouvian M, et al. Sustained rhythmic brain activity underlies visual motion perception in zebrafish. Cell Rep 2016;17:1098–1112.
19. Huang YY, Neuhauss SC. The optokinetic response in zebrafish and its applications. Front Biosci 2008;13:1899–1916.
20. Keary N, Ruploh T, Voss J, et al. Oscillating magnetic field disrupts magnetic orientation in zebra finches, *Taeniopygia guttata*. Front Zool 2009;6:1–7.
21. Park JS, Ryu JH, Choi TI, et al. Innate color preference of zebrafish and its use in behavioral analyses. Mol Cells 2016;39:750–755.
22. Voss J, Bischof HJ. Eye movements of laterally eyed birds are not independent. J Exp Biol 2009;212:1568–1575.
23. Gooding DC, Basso MA. The tell-tale tasks: a review of saccadic research in psychiatric patient populations. Brain Cogn 2008;68: 371–390.
24. Matthysse S, Holzman PS, Gusella JF, et al. Linkage of eye movement dysfunction to chromosome 6p in schizophrenia: additional evidence. American journal of medical genetics part B: neuropsychiatric. Genetics 2004;128:30–36.
25. Ma M, Ramirez AD, Wang T, et al. Zebrafish dscaml1 deficiency impairs retinal patterning and oculomotor function. J Neurosci 2020; 40:143–158.
26. Gudmundsson S, Wilbe M, Filipek-Górniok B, et al. TAF1, associated with intellectual disability in humans, is essential for embryogenesis and regulates neurodevelopmental processes in zebrafish. Sci Rep 2019;9:10730.
27. Zheng J, Long F, Cao X, et al. Knockout of Katnal2 leads to autism-like behaviors and developmental delay in zebrafish. Int J Mol Sci 2022;23:8389.
28. Huang YY, Rinner O, Hedinger P, et al. Oculomotor instabilities in zebrafish mutant belladonna: a behavioral model for congenital nystagmus caused by axonal misrouting. J Neurosci 2006;26:9873–9880.
29. Seth A, Culverwell J, Walkowicz M, et al. Belladonna/(lhx2) is required for neural patterning and midline axon guidance in the zebrafish forebrain. Development 2006;133:725-735.
30. Chinn GA, Hirokawa KE, Chuang TM, et al. Agenesis of the corpus callosum due to defective glial wedge formation in Lhx2 mutant mice. Cereb Cortex 2015;25:2707–2718.
31. Staley JP, Guthrie C. Mechanical devices of the spliceosome: motors, clocks, springs, and things. Cell 1998;92:315–326.
32. Wahl MC, Will CL, Lührmann R. The spliceosome: design principles of a dynamic RNP machine. Cell 2009 Feb;136:701–718.
33. Nakagawa O, Arnold M, Nakagawa M, et al. Centronuclear myopathy in mice lacking a novel muscle-specific protein kinase transcriptionally regulated by MEF2. Genes Dev 2005;19:2066–2077.
34. Vogel P, Read RW, Hansen GM, Powell DR. Histopathology is required to identify and characterize myopathies in high-throughput phenotype screening of genetically engineered mice. Vet Pathol 2021;58:1158–1171.
35. Seo MH, Yeo S. Association between decreased *Srpk3* expression and increased substantia Nigra alpha-synuclein level in an MPTP-induced Parkinson's disease mouse model. Mol Neurobiol 2023;60: 780–788.
36. Price ER, Mager EM. The effects of exposure to crude oil or PAHs on fish swim bladder development and function. Comp Biochem Physiol C Toxicol Pharmacol 2020;1:108853.
37. Lindsey BW, Smith FM, Croll RP. From inflation to flotation: contribution of the swimbladder to whole-body density and swimming depth during development of the zebrafish (*Danio rerio*). Zebrafish 2010;7: 85–96.
38. May M, Hwang KS, Miles J, et al. ZC4H2, an XLID gene, is required for the generation of a specific subset of CNS interneurons. Hum Mol Genet 2015;24:4848–4861.
39. Lee YR, Khan K, Armfield-Uhas K, et al. Mutations in FAM50A suggest that Armfield XLID syndrome is a spliceosomopathy. Nat Commun 2020;11:3698.
40. Lee YR, Kim SH, Ben-Mahmoud A, et al. Eif2b3 mutants recapitulate phenotypes of vanishing white matter disease and validate novel disease alleles in zebrafish. Hum Mol Genet 2021;30:331–342.
41. Caldani S, Gerard CL, Peyre H, Bucci MP. Pursuit eye movements in dyslexic children: evidence for an immaturity of brain oculomotor structures? J Eye Mov Res 2020;13:13.
42. Goldberg MC, Lasker AG, Zee DS, et al. Deficits in the initiation of eye movements in the absence of a visual target in adolescents with high functioning autism. Neuropsychologia 2002;40:2039–2049.
43. Lee MM, Arrenberg AB, Aksay ER. A structural and genotypic scaffold underlying temporal integration. J Neurosci 2015;35: 7903–7920.
44. Vishwanathan A, Daie K, Ramirez AD, et al. Electron microscopic reconstruction of functionally identified cells in a neural integrator. Curr Biol 2017;27:2137–2147.
45. Cannon SC, Robinson DA. Loss of the neural integrator of the oculomotor system from brain stem lesions in monkey. J Neurophysiol 1987;57:1383–1409.
46. Lencer R, Mills LJ, Alliey-Rodriguez N, et al. 11. Extended association studies of smooth pursuit and Antisaccade eye movements: findings from the B-SNIP study. Schizophr Bull 2017;43:S10–S11.
47. Hibi M, Matsuda K, Takeuchi M, et al. Evolutionary mechanisms that generate morphology and neural-circuit diversity of the cerebellum. Dev Growth Differ 2017;59:228–243.
48. Mueller T, Wullimann MF. Anatomy of neurogenesis in the early zebrafish brain. Dev Brain Res 2003;140:137–155.

49. Wullimann MF, Mueller T. Teleostean and mammalian forebrains contrasted: evidence from genes to behavior. J Comp Neurol 2004; 4:427–428.

50. Kebschull JM, Richman EB, Ringach N, et al. Cerebellar nuclei evolved by repeatedly duplicating a conserved cell-type set. Science 2020;370:eabd5059.

51. Chang W, Pedroni A, Köster RW, et al. Purkinje cells located in the adult zebrafish valvula cerebelli exhibit variable functional responses. Sci Rep 2021;11:18408.

52. Kim TY, Roychaudhury A, Kim HT, et al. Impairments of cerebellar structure and function in a zebrafish KO of neuropsychiatric risk gene znf536. Transl Psychiatry 2024;14:82.

53. Singh S, Garge S. Agenesis of the corpus callosum. J Pediatr Neurosci 2010;5:83–85.

54. Bitanihirwe BK, Lizano P, Woo TU. Deconstructing the functional neuroanatomy of the choroid plexus: an ontogenetic perspective for studying neurodevelopmental and neuropsychiatric disorders. Mol Psychiatry 2022;27:3573–3582.